Journal of the Korean Physical Society, Vol. 59, No. 2, August 2011, pp. 1649∼1653

# Fission Physics and Cross Section Measurements with a Lead Slowing down Spectrometer

Y. Danon,* R. Block (emeritus), J. Thompson and C. Romano†
*Rensselaer Polytechnic Institute, Troy, NY 12180, USA*

(Received 26 April 2010)

A Lead Slowing Down Spectrometer (LSDS) provides a high neutron flux environment that enables measurements of small samples (∼$\mu$g) or samples with small cross sections (tens of $\mu$b). The LSDS at Rensselaer Polytechnic Institute (RPI) was previously used for fission cross section measurements and for studies of methods for assay of used nuclear fuel. The effective energy range for the LSDS is 0.1 eV to 10 keV with energy resolution of about 35%. Two new LSDS applications were recently developed at RPI; the first enables simultaneous measurements of the fission cross section and fission fragment mass and energy distributions as a function of the incident neutron energy. The second enables measurements of the $(n,\alpha)$ and $(n,p)$ cross sections for materials with a positive Q value for these reactions. Fission measurements of $^{252}$Cf, $^{235}$U, and $^{239}$Pu were completed and provide information on fission fragment and energy distributions in resonance clusters. Measurements of the $(n,\alpha)$ cross section for $^{147,149}$Sm were completed and compared to previously measured data. The new data indicate that the existing evaluations need to be adjusted.

PACS numbers: 25.40.-h, 25.85.Ec
Keywords: ND2010, Nuclear data, Lead slowing down spectrometer, Fission, Cross section
DOI: 10.3938/jkps.59.1649

## I. INTRODUCTION

A Lead Slowing Down Spectrometer (LSDS) is a large cube of lead with a pulsed fast neutron source in its center [1]. The neutron slowing down process results in a high neutron flux with about 35% energy resolution in the energy range between 0.1 eV to 10 keV. The relation between the slowing down time $t$ and the mean neutron energy $E$ in the LSDS is very similar to the expression used for neutron time-of-flight experiments:

$$E = \frac{K}{(t - t_0)^2}. \quad (1)$$

The constants $K$and $t_0$ depend on the size and purity of the lead cube; for the RPI LSDS with cube side of 180 cm, $K$ =165 keV*$\mu$s$^2$ and $t_0$ = 0.3 $\mu$s [1]. To perform a fission cross section measurement, a detector is placed in the LSDS and the reaction rate $R$ is recorded as a function of the slowing-down-time. The fission cross section at energy $E_{\rm i}$ corresponding to slowing down time $t_{\rm i}$ recorded in channel $i$ is given by [2]:

$$\sigma_f(E_i) = \frac{R(E_i)}{N\eta\varphi(E_i)\Delta E_i}, \quad (2)$$

where $N$ is the number of atoms in the sample, $\eta$ is the detector efficiency, $\varphi(E_{\rm i})$ is the neutron flux per eV at energy $E_{\rm i}$, and $\Delta E_{\rm i}$ is the energy width of channel $i$. Measurement of other cross sections such as $(n,\alpha)$ and $(n,p)$ is done a similar way.

In the US there are currently two spectrometers; one at Rensselaer Polytechnic Institute (RPI), and another at Los Alamos National Laboratory (LANL). Previous fission cross section measurements at the RPI and LANL LSDSs can be found in previous publications, for example [2-5]. Other LSDS devices were also constructed in Russia [6] and Japan [7]. We report on two new applications of the LSDS; the first provides more information about physics of the fission process obtained from simultaneous measurements of the fission cross section and fission fragment mass and energy distributions as a function of the incident neutron energy. The second enables measurements of the $(n,\alpha)$ and $(n,p)$ cross section on materials with a positive Q value for these reactions.

In order to measure the fission fragment mass and energy a double gridded fission chamber was constructed and placed in the LSDS about 40 cm from the neutron source. The design of the chamber and associated electronics allowed relatively fast recovery from the very strong gamma flash to allow measurements up to 2 keV.

Compensated detectors were developed to allow measurements of the alphas and protons emitted from neutron interactions with the sample material while operating in the high neutron and gamma radiation environment inside the LSDS.

*E-mail: danony@rpi.edu
†Permanent address: Oak Ridge National Laboratory, Oak Ridge, USA

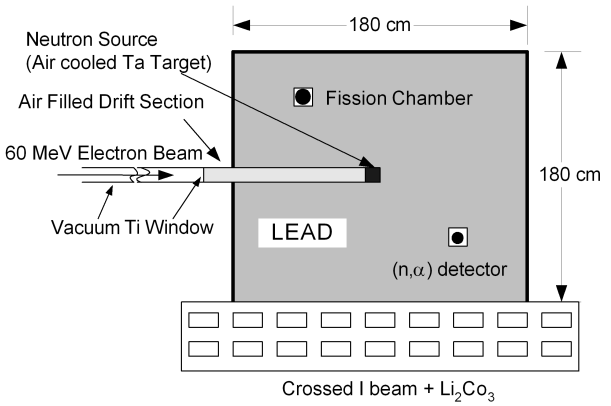


Fig. 1. The LSDS setup showing the electron beam entrance from the left, neutron production target, and detector locations. To prevent neutron room return the LSDS is covered with cadmium and shielded with $Li_2CO_3$ on the bottom.

## II. EXPERIMENTAL SETUP

The LSDS setup at RPI is shown in Fig. 1, the electron beam is incident from the left hitting an air cooled tantalum target placed in the center of a high purity lead cube. There are two detector positions and data can be measured for two detectors in both locations simultaneously.

### 1. Fission Chamber

The fission chamber is described in detail in Refs. 8 - 11. It is a double gridded fission chamber with a sample deposited on thin polyamide (∼250 nm) backing positioned on a cathode at the center of the chamber. A photo of the internals of the fission chamber is shown in Fig. 2.

This setup enables measurement of the energy deposited by the two fission fragments in the gas. The signal from the cathode is used for timing and to trigger data collection from the grids and anodes. The data from the two grids and anodes is used for obtaining the fragment energy and emission angle. These values are then used to correct for the energy loss in the sample and calculate the post neutron emission fission fragment mass and energy. Using published data for neutron emission as a function of fission fragment total kinetic energy (TKE) and mass (see Ref. 12) it is possible to obtain the preneutron emission mass and energy distributions.

Data acquisition is accomplished by connecting the fission chambers' grid and anode signals to a preamplifier with a time constant of 500 ns that matches the charge collection time of about 400 ns. The signal is then shaped with a 200 ns amplifier and the pulse height is digitized using ADCs [9].

Data was collected for 0.41 ng of $^{252}$C (outside the LSDS) and was used to test the setup and qualify it by comparing to published data [10]. Data for 25.3 $\mu$g of $^{235}$U and 26.9 $\mu$g of $^{239}$Pu was collected with the LSDS operating at a pulse rate of 180 Hz, electron energy of

Fig. 2. (Color online) A photo of the double gridded fission chambers showing the cathode with the sample in the center (with guard rings above and below) and the two grids and anodes.

∼58 MeV and average current of ∼8 $\mu$A. Although the sample size is small, the high neutron flux in the LSDS provided enough events to have small counting statistics errors in a short run time of a few hours.

### 2. Detectors for $(n,\alpha)$ and $(n,p)$ measurements

The primary effort in measurements of $(n,\alpha)$ and $(n,p)$ cross sections was related to finding the appropriate detectors. This is necessary because the LSDS environment includes a very intense gamma flash and high neutron (and gamma) flux that can damage the detectors or paralyze the system. The signal obtained from alpha energy deposition in the detector is much smaller relative to fission and thus the noise from the high neutron and gamma flux environment are more problematic in this type of measurement. The proximity of the detector to the neutron producing tantalum target results in an intense gamma flash that induces a large pulse that paralyzes the electronics and thus induces a long dead time. It is important to note that according to Eq. (1) after a slowing down time of 1 $\mu$s the mean energy in the LSDS is about 97 keV and in 4 $\mu$s it drops below 10 keV. It is thus very important to keep the recovery time short in order to be able to obtain data above 10 keV.

In order to reduce the gamma flash dead time, com-

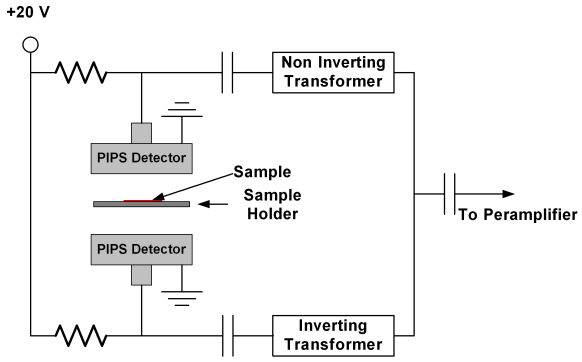


Fig. 3. (Color online) A diagram of the two PIPS detectors in a compensating configuration. This configuration enabled measurements of the sample signal and background using the sum signal.

pensated detectors are used. Several compensated detector concepts were examined including: solar cells, ionization chambers [13], GEM based detectors and solid stated Passivated Implanted Planar Silicon (PIPS) detectors [14]. The concept that yielded the best result was the PIPS detectors and this is primarily because of the large signal to noise ratio. However these detectors suffer degradation during the experiment and can become useless after several hours in the LSDS. During the detector degradation process it was observed that the pulse height and resolution degrades, but the signal in this detector is high relative to the noise and with proper configuration the detection efficiency remains constant. The configuration used included two detectors; the signal of one was passively inverted and summed with the second detector to provide compensation during the gamma flash. The sample faced the non inverted detector such that during the measurement that detector measured the alphas emitted from the sample and the second measured the background. This was important in order to make sure that capture gammas from the strong 0.097 eV resonance in $^{149}$Sm that possibly interact with the detector can be subtracted from the alpha signal. During the gamma flash both detectors had about the same response and thus their signal summed to zero (or a small value).

The sum signal was fed to an Aquiris DC4404 12 bit digitizer and a bipolar signal was recorded such that the polarity allowed to distinguish the two detectors and thus provide simultaneous measurements of the signal and background while using a compensated detector.

## III. RESULTS

### 1. Fission Fragment Spectroscopy

Simultaneous measurements of the fission cross section and the fission fragment mass and energy distributions as a function of incident neutron energy were completed for $^{235}$U and $^{239}$Pu. The high neutron flux in the LSDS allowed for short data collection time of a few hours and provided data from 0.1 eV to about 2 keV. The data

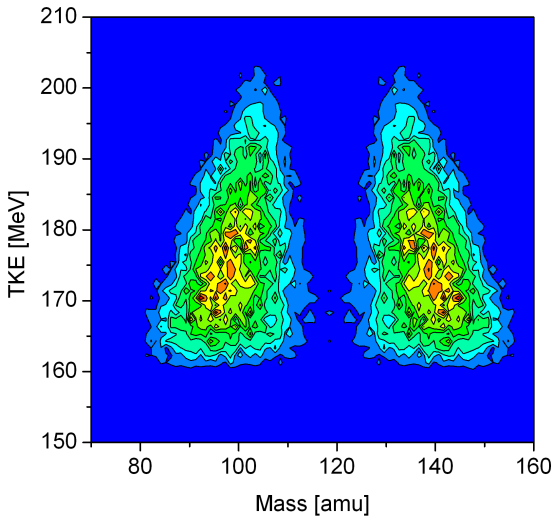


Fig. 4. (Color online) $^{239}$Pu preneutron emission fission fragment yield as function of TKA and mass in the thermal region ($E_n < 0.1$ eV).

below 0.1 eV has poor resolution with respect to the incident neutron energy but can be used to obtain data for an average thermal spectrum. Data reduction procedure and results for $^{235}$U were outlined in detail in Refs. 9 and 10. A contour plot of the $^{239}$Pu preneutron emission fission fragment yield as a function of the TKA and mass for incident neutron energy in the thermal region ($E_n <$ 0.1) is shown in Fig. 4.

Similar data is available for other incident neutron energies and demonstrate the capability to study fission symmetry and variations in TKE as a function of incident neutron energy as previously demonstrated for $^{235}$U [9]. Figure 5 shows the $^{239}$Pu fission cross section as measured in the LSDS and the energy regions limits used to construct the mass distributions shown in Fig. 6. The measured cross section shows the effect of the broad energy resolution of the LSDS indicating that with the exception of the low energy resonances, the selected energy regions can only cover resonance clusters.

The prenuetron emission mass distributions in Fig. 6 show variations as a function of incident neutron energy. Note the good statistics in these plots which result from the intense flux inside the LSDS. Region 9 exhibits strong variations in the yield in the mass range of 100 - 110 and 130 - 140 amu which is currently unexplained and warrants further investigation. Similar variation was also observed in one region of the $^{235}$U data [9].

### 2. $^{147,149}$Sm $(n,\alpha)$ Cross Section

The isotopes $^{147}$Sm and $^{149}$Sm both have positive Q value for the $(n,\alpha)$ reaction which means that there is no threshold for the reaction. Both reactions emit an energetic 9 MeV alpha particle which easily escapes a

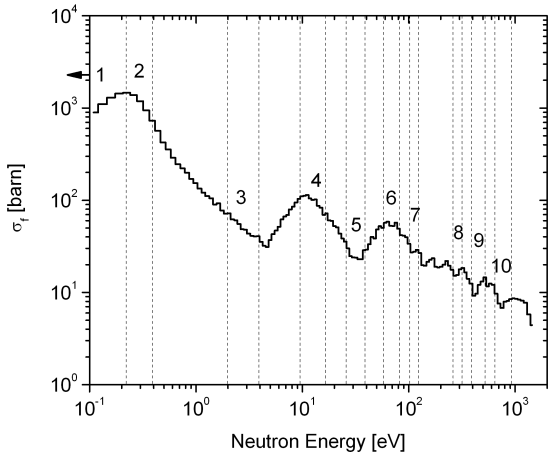


Fig. 5. Measured $^{239}$Pu fission cross section and the energy regions that were set in order to study the variation in fission fragment mass and TKE.

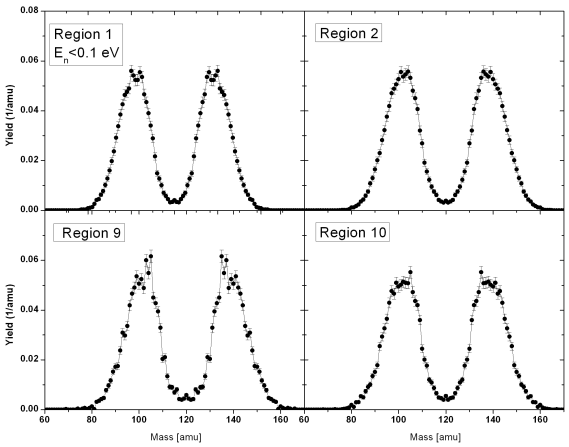


Fig. 6. $^{239}$Pu preneutron emission fission fragment mass distributions for several incident neutron energy regions corresponding to Fig. 5.

relatively thick sample thus helping to reduce degradation of the detection efficiency.

Samples of $^{147}$Sm and $^{149}$Sm were prepared by dissolving $Sm_2O_3$ in nitric acid. Solutions of enriched $^{147}$Sm (98.03%) and $^{149}$Sm (97.67%) isotopes were stippled onto a thin backing to form nitrate samples containing 8.25 mg $^{147}$Sm and 7.99 mg $^{149}$Sm with sample area of about 1.4 cm$^2$. As discussed in section 2.2 the data was analyzed to separate negative from positive pulses to allow background subtraction. The $^{147}$Sm data was reduced to cross section and was normalized to ENDF/B-7.0 [15] broadened to the LSDS resolution in the energy range from 3 – 300 eV In this energy range the ENDF cross section overlaps a newer high resolution measurement [16] which was not included in the evaluation.

The $^{149}$Sm data was analyzed using the detection efficiency obtained for the $^{147}$Sm sample. The cross sections for both isotopes are plotted in Fig. 7. In both cases the data is considerably different from the evaluations. For the case of $^{147}$Sm there is good agreement to Ref. 16. The $^{147}$Sm thermal cross section agrees better with the JENDL 3.3 evaluation [18] and is higher than Ref. 19. For $^{149}$Sm the cross section is in good agreement with the measurements of Refs. 20 - 22 and in the thermal region it is closer to Ref. 23 disagreeing with the two evaluations.

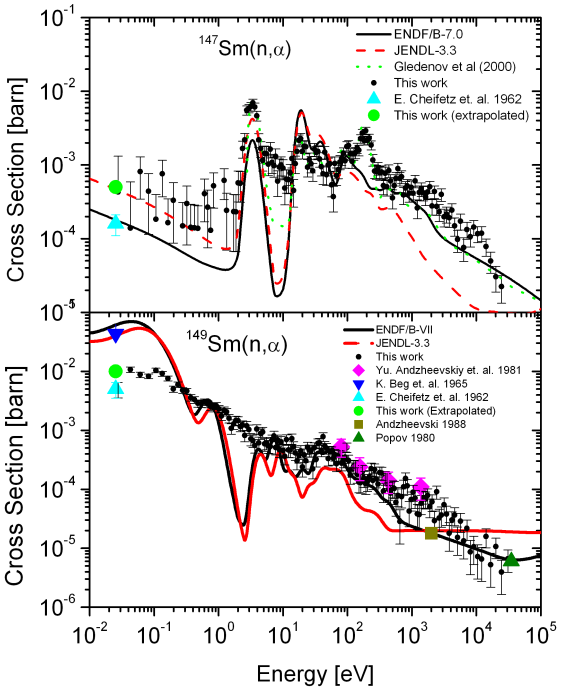


Fig. 7. (Color online) $^{147,149}$Sm $(n,\alpha)$ cross section measured with the LSDS at RPI compared with other data and current evaluations broadened to the LSDS energy resolution.

## IV. CONCLUSIONS

The LSDS provides a high flux environment that enables neutron induced reaction measurements of small samples ($<\mu$g) or samples with small cross sections (tens of micro barns). Although in its useful energy range between 0.1 eV and 10 keV the LSDS has an energy resolution of about 35%, it can be used to obtained useful data in the resonance region.

A method for simultaneous measurements of the fission cross section and fission fragment mass and energy distributions as a function of incident neutron energy was developed and used for measurements of $^{235}$U and $^{239}$Pu samples. The high flux environment allows the use of small mass samples and requires a relatively short experiment time. This capability enables measurement on actinides that are available in small quantities.

Data presented here and in Refs. 9 and 10 demonstrate the ability to extract information on the variations

of mass and energy distributions with incident neutron energy in the resonance region. Fission yield data as a function of TKE and fragment mass were measured and currently, in conjunction with advanced fission models [17], these data can be used to predict the impact on other fission observables.

Methods were developed to perform $(n,\alpha)$ and $(n,p)$ cross section measurements with the LSDS. A system of solid-state PIPS detectors was used to construct a compensated detector and enabled simultaneous measurement of the alpha particles and the neutron and gamma induced background. Measurements of $^{147,149}$Sm sample demonstrate the ability of this system to provide new cross section data to improve current evaluated data files. Improvements to the method by using other types of detectors and methods to eliminate background from radioactive samples are under development.

## ACKNOWLEDGMENTS

The authors would also like to thank the DOE for their funding of this research, grant numbers: DE-FG03-03NA00079, DE-FG52-06NA26202, DE-FG52-09NA29453.

## REFERENCES

[1] R. E. Slovacek, D. S. Cramer, E. B. Bean, R. W. Hockenbury, J. R. Valentine and R. C. Block, Nucl. Sci. Eng. **62**, 455 (1977).
[2] Y. Danon, R. E. Slovacek, R. C Block, R. W. Lougheed, R. W. Hoff and M. S. Moore, Nucl. Sci. Eng. **109**, 341 (1991).
[3] H. T. Maguire, C. R. S. Stopa, R. C. Block, D R. Harris, R E. Slovacek, J. W. T. Dabbs, R. J. Dougan, R. W. Hoff and R. W. Lougheed, Nucl. Sci. Eng. **89**, 293 (1985).
[4] B. Alam, R. C. Block, R. R. Slovacek and R. W. Hoff, Nucl. Sci and Eng. **22**, 267 (1988).
[5] D. Rochman *et al.*, Nucl. Instrum. Methods Phys. Res., Sect. A **564**, 400 (2006).
[6] A. A. Alexeev, A. A. Bergman, A. N. Volkov, O. N. Goncharenko, A. P. Zhukov, A. D. Perekrestenko and N. M. Sobolevsky, in *Proceedings of XVI Inter. Works. on Phys. of Nucl. Fission* (Obninsk, Russia, 2003).
[7] K. Katsuhei, Y. Shuji, Y. Akihiro, N. Yoshihiro, F. Yoshiaki, K. Satoshi and K. Itsuro, Nucl. Instrum. Methods Phys. Res., Sect. A **385**, 145 (1997).
[8] C. Romano, Y. Danon, R. Block, E. Blain and E. Bond, in *Proceedings of the Inter. Conf. on Nucl. Data for Sci. and Techn.* (Nice, France, 2007), (EDP Sciences, 2008), p. 371.
[9] C. Romano, Y. Danon, R. Block, J. Thompson, E. Blain and E. Bond, Phys. Rev. C **81**, 014607 (2010).
[10] R. Catherine, *PhD Thesis Dissertation*, Rensselaer Polytechnic Institute, Troy, NY, 2009.
[11] C. Budtz-Jorgensen and H.-H. Knitter, Nucl. Instrum. Methods **223**, 295 (1984).
[12] E. E. Maslin, A. L. Rodgers and W. G. F. Core, Phys. Rev. **164**, 1520 (1967).
[13] C. Romano *et al.*, Nucl. Instrum. Methods Phys. Res., Sect. A **562**, 771 (2006).
[14] The detector is produced by Canberra, http://www.canberra.com/.
[15] M. B. CHADWICK *et al.*, Nucl. Data Sheets **107**, 12, 2931, (2006).
[16] Yu. M. Gledenov, P. E. Koehler, J. Andrzejewski, K. H. Guber and T. Rauscher, Phys. Rev. C **62**, 042801(R) (2000).
[17] P. Talou and T. Kawano, *CNR*09 - Second Inter. Works. on Compound Nucl. React. and Related Topics*, EPJ Web of Conf. **2**, (2010), DOI:10.1051/epjconf/20100208005.
[18] K. Shibata *et al.*, J. Nucl. Sci. Technol. **39**, 1125 (2002).
[19] E. Cheifetz, J. Gilat, A. L. Yavin and S. G. Cohen, Phys. Lett. **1**, 289 (1962).
[20] Yu. Andzheevsky, V. P. Vertebny, V. K. Tkhan, V. A. Vtyurin, A. L. Kirilyuk and Yu. P. Popov, Yad. Fiz. **48**, 20 (1988).
[21] J. Andrezeewsky, V. K. Thang, V. A. Vtyurin, A. Koreiwo, Yu. P. Popov and M. Stempinsky, Yad. Fiz. **32**, 1496 (1980).
[22] Yu. P. Popov, V. I. Salatskij and G. Khuukhenkhuu, Yad. Fiz. **32**, 893 (1980).
[23] K. Beg and R. D. Macfarlane, Bull. Am. Phys. Soc. **10**, 724, EG8 (1965).